

Importance of Fermi surface and magnetic interactions for the superconducting dome in electron doped FeSe intercalates

Makoto Shimizu,¹ Nayuta Takemori,² Daniel Guterding,³ and Harald O. Jeschke²

¹*Department of Physics, Okayama University, Okayama 700-8530, Japan*

²*Research Institute for Interdisciplinary Science, Okayama University, Okayama 700-8530, Japan*

³*Fachbereich Mathematik, Naturwissenschaften und Datenverarbeitung, Technische Hochschule Mittelhessen, Wilhelm-Leuschner-Straße 13, 61169 Friedberg, Germany*

The van-der-Waals gap of iron chalcogenide superconductors can be intercalated with a variety of inorganic and organic compounds that modify the electron doping level of the iron layers. In $\text{Li}_x(\text{C}_3\text{N}_2\text{H}_{10})_{0.37}\text{FeSe}$, a dome in the superconducting transition temperature T_c has been reported to occur in the doping range of $x = 0.06$ to $x = 0.68$. We use a combination of density functional theory and spin fluctuation theory to capture the evolution of superconducting transition temperatures theoretically. We clearly demonstrate how the changing electronic structure supports an increasing superconducting T_c . The suppression of T_c at high doping levels can, however, only be understood by analyzing the magnetic tendencies, which evolve from stripe-type at low doping to bicollinear at high doping.

Introduction.— Iron chalcogenide superconductors, while structurally simple, have emerged as one of the most interesting and electronically most complicated of the various families of iron-based superconductors^{1–3}. FeSe, in particular, is intensely studied due to its nematic phase which occurs in a very large temperature range⁴ and due to its peculiar electronic structure that is not correctly captured by any known electronic structure technique⁵. After the discovery of superconducting FeSe⁶ it was realized that the superconducting transition temperatures can be significantly enhanced if the van der Waals gap between the iron selenium layers is intercalated with alkali metal ions, for example by the ammonia technique^{7–10} or directly in the structurally complicated $A_x\text{Fe}_{2-y}\text{Se}_2$ type of compounds with $A = \text{K}, \text{Rb}, \text{Cs}$ ^{11,12}. Further possibilities are completely inorganic lithium hydroxide intercalates^{13,14}, and alkali metal intercalates stabilized by organic solvents¹⁵. Not only FeSe but also FeS¹⁶ and $\text{FeSe}_{1-x}\text{Te}_x$ ^{17,18} can be intercalated.

At least three tuning parameters have been identified that provide control over the superconducting transition temperature: Pressure can increase the T_c of bulk FeSe from 8 K at ambient pressure to 36.7 K¹⁹. By electron doping via lithium and ammonia intercalation, T_c up to 55 K can be reached¹⁰. The spacing between FeSe layers can be systematically increased using amines of increasing size, like ethylenediamine ($\text{C}_2\text{H}_8\text{N}_2$)^{15,20}, 2-phenethylamine ($\text{C}_3\text{H}_{11}\text{N}$)²¹, diaminopropane ($\text{C}_3\text{H}_{10}\text{N}_2$)^{20,22}, hexamethylenediamine ($\text{C}_6\text{H}_{16}\text{N}_2$)^{23,24}, and T_c up to 41 K has been observed²⁴.

Tuning parameters can also be combined, for example by pressurizing doped FeSe intercalates^{25–28}. When parameters like pressure or doping, which can be varied continuously, are tuned away from their optimal values, characteristic superconducting domes are observed^{25–29}.

Here, we are interested in finding microscopic explanations for superconducting domes, also in the hope of discovering ways to manipulate and increase transition temperatures. Theoretically, superconductivity in iron-

based materials has been tackled from a weak coupling perspective, describing Fermi surface instabilities that lead to superconductivity via spin fluctuations^{30–32}, and from a strong coupling picture by considering these materials as doped Mott insulators, where superconductivity is obtained from approximately solved t - J models^{33–35}. However, capturing superconducting T_c trends continues to be a theoretical challenge³⁶. Within a spin fluctuation scenario, the T_c increase with doping has been explained for lithium ammonia intercalated FeSe³⁷, and for FeS, a pressure induced double dome was captured³⁸. The dispute between itinerant and localized electron pictures is ongoing, and while some iron-based superconductor families, like 1111, are more itinerant, others, like hole doped 122 and iron chalcogenides are more localized. In fact, superconductivity can be shown to depend both on Fermi surface shape and antiferromagnetic exchange³⁹. Even in the absence of a magnetic ground state, the nature of the magnetic exchange has important implications for nematicity and superconductivity in FeSe⁴⁰ and for the differences between iron pnictides and germanides⁴¹.

In this Rapid Communication, we will focus on the lithium diaminopropane intercalated material $\text{Li}_x(\text{C}_3\text{N}_2\text{H}_{10})_{0.37}\text{FeSe}$ where charge doping has been controlled experimentally in a wide range $0.06 \leq x \leq 0.68$ ²². We will work both in the itinerant scenario by applying spin fluctuation theory and in the localized picture by working out the consequences of the Heisenberg interactions. We will show that the underdoped side of the superconducting dome can be well understood based on Fermi surfaces, but in order to explain the decreasing T_c at high doping, we need to evoke the high energy argument that, with increasing carrier density, magnetic interactions mutate from FeSe-like to FeTe-like.

Methods.— We study the electronic structure of $\text{Li}_x(\text{C}_3\text{N}_2\text{H}_{10})_{0.5}\text{FeSe}$ as a function of doping by performing a series of density functional theory (DFT) calculations within the full-potential local orbital (FPLO)⁴² basis, using the generalized gradient approximation (GGA)

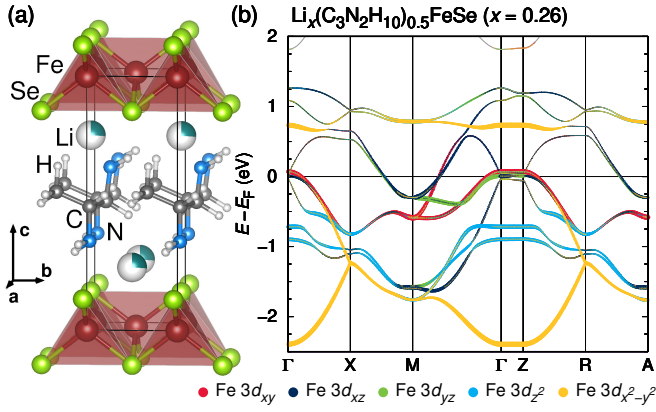


FIG. 1. (a) Crystal structure of $\text{Li}_x(\text{C}_3\text{N}_2\text{H}_{10})_{0.5}\text{FeSe}$; the Li position is only 26% occupied, indicated by partial coloring. (b) Corresponding bands near the Fermi level E_F with Fe 3d orbital weights.

exchange correlation functional⁴³ and $24 \times 24 \times 24$ k -mesh. We construct tight-binding models including all ten Fe 3d orbitals using projective Wannier functions⁴⁴. Using the glide reflection unfolding technique⁴⁵, we turn the ten-band into a five-band model. We calculate the noninteracting susceptibility χ_0 on a $50 \times 50 \times 10$ q -mesh. We employ the random phase approximation (RPA) to calculate spin and charge susceptibilities and solve a gap equation to obtain pairing symmetry Δ and eigenvalue λ ^{46,47}. On the other hand, we use the energy mapping method to measure the exchange interactions of $\text{Li}_x(\text{C}_3\text{N}_2\text{H}_{10})_{0.5}\text{FeSe}$ ^{41,48,49} and iterative minimization to find ground state spin configurations for the calculated Hamiltonians^{50,51}.

Results. - We first generate a sequence of crystal structures for $\text{Li}_x(\text{C}_3\text{N}_2\text{H}_{10})_{0.37}\text{FeSe}$ based on the structural data determined by Sun *et al.*²². We smoothly interpolate the structural data for the lattice parameters and the FeSe layer (see Ref. 51 for details, in particular Fig. S1) and simplify the disordered diaminopropane molecules to a single molecule per two FeSe, yielding the composition $\text{Li}_x(\text{C}_3\text{N}_2\text{H}_{10})_{0.5}\text{FeSe}$ shown in Figure 1 (a). We mount the $\text{C}_3\text{N}_2\text{H}_{10}$ molecule with fixed geometry into the entire structure sequence, since bond lengths and angles of a neutral molecule should not be affected by the charging and contraction of the FeSe layer (see Ref. 51 for further details). An example of the DFT electronic structure with Fe 3d weights is shown in Figure 1 (b). Calculations for the complete sequence of structures without diaminopropane molecule, in $P4/mnn$ symmetry, yield similar results⁵¹.

We first quantify the charge doping by integration of Fe 3d total and partial electron densities. We find that the charge $-xe$ provided by Li_x^+ is indeed fully doping the Fe plane; Fe charge evolves almost linearly from $n_{3d}^{\text{total}} = 6.06$ to 6.65 in the interval $0.06 < x < 0.68$ (see Ref. 51, Fig. S2). The orbital with strongest charge increase is d_{xy} , followed by d_{xz}/d_{yz} .

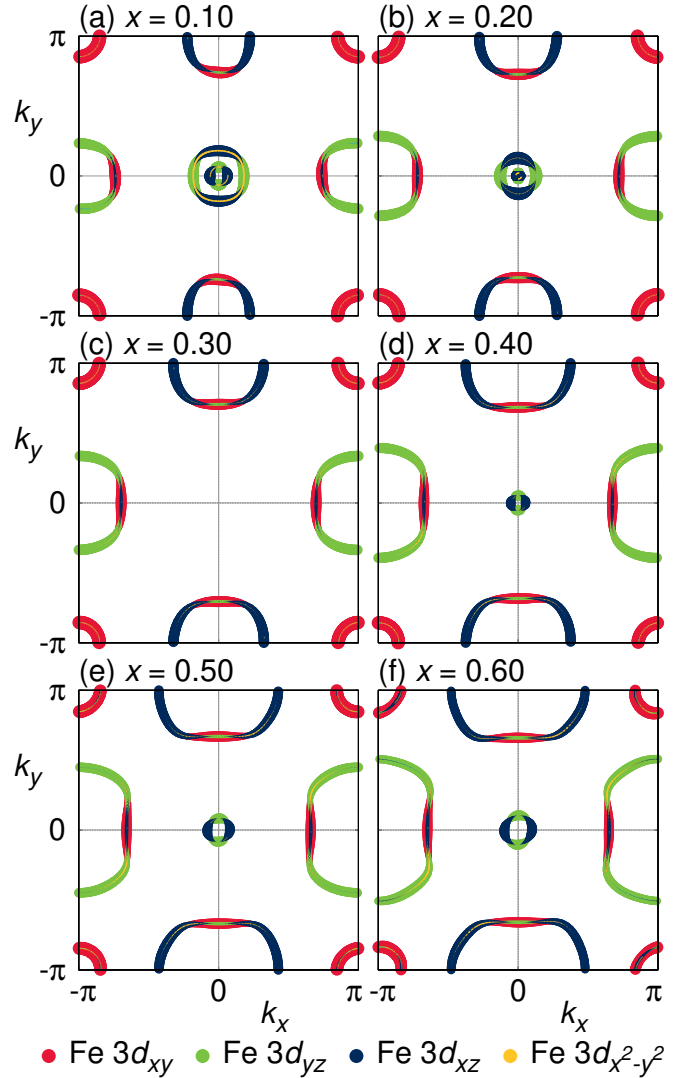


FIG. 2. Evolution of the Fermi surface of $\text{Li}_x(\text{C}_3\text{N}_2\text{H}_{10})_{0.5}\text{FeSe}$ at $k_z = 0$ with doping. The Fe 3d orbital weights are indicated by color. Orbital weight of Fe $3d_{z^2}$ at the Fermi level is nearly negligible.

The decisive factor in spin fluctuation theory is Fermi surfaces. We show in Figure 2 the unfolded one iron Fermi surfaces of $\text{Li}_x(\text{C}_3\text{N}_2\text{H}_{10})_{0.5}\text{FeSe}$ for six doping levels (see Fig. S3 of Ref. 51 for the same without $\text{C}_3\text{N}_2\text{H}_{10}$ molecules). First of all, we note that the overall number and size of Fermi surface pockets are in good agreement with those observed by angle resolved photoemission in the related FeSe intercalates $(\text{Li}_{0.84}\text{Fe}_{0.16})\text{OHFe}_{0.98}\text{Se}$ and $(\text{Tl,Rb})_x\text{Fe}_{2-y}\text{Se}_2$ (see Fig. 1 of Ref. 52). Even though we do not know the precise doping levels of those compounds, the overall similarity in the Fermi surfaces gives us confidence that for $\text{Li}_x(\text{C}_3\text{N}_2\text{H}_{10})_{0.5}\text{FeSe}$, we can avoid the difficulties of bulk FeSe where size and symmetry of Fermi surfaces are captured neither by DFT nor its extensions. Note, also, that DFT+DMFT, as applied in Ref. 22, has only a small effect on the Fermi surface

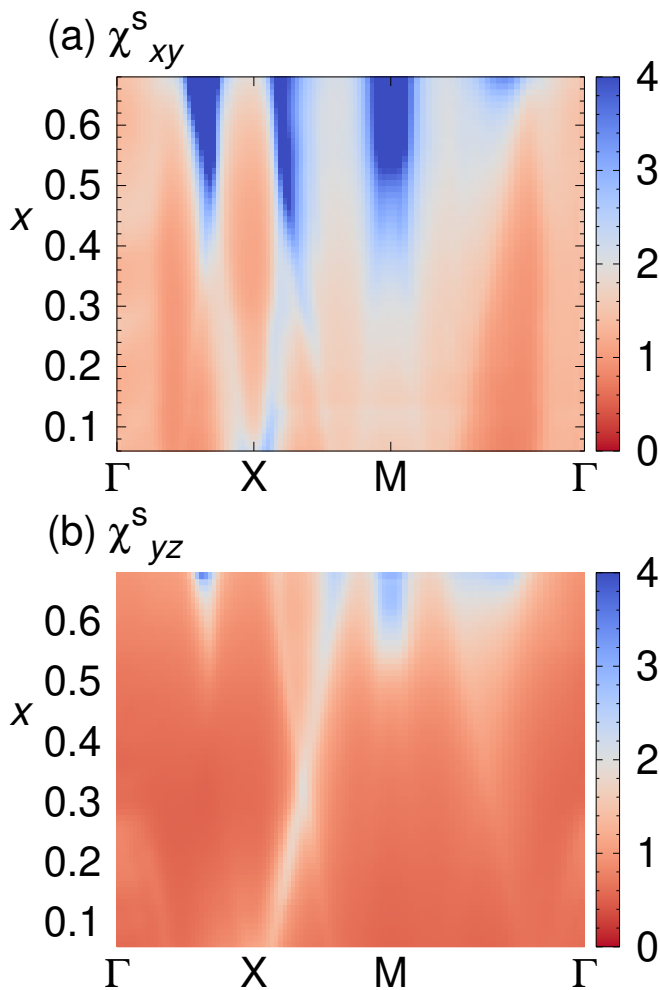


FIG. 3. Diagonal elements of the spin susceptibility as a function of momentum vector and doping.

of $\text{Li}_x(\text{C}_3\text{N}_2\text{H}_{10})_{0.5}\text{FeSe}$. Thus, the DFT Fermi surfaces are a reasonable starting point for the description of the material. We would like to stress that we take advantage of the fact that in contrast to bulk FeSe where superconductivity develops out of a paramagnetic nematic phase with strong fluctuating magnetic moments which is not fully captured by DFT or DFT+DMFT, magnetic tendencies of FeSe intercalates are more conventional and therefore amenable to the electronic structure methods we employ here.

The dominant feature in the Fermi surface evolution with doping is the strong growth of the large angular electron pockets around the X and Y points in the one iron Brillouin zone (BZ). They have combined d_{xy} and d_{xz}/d_{yz} character. The hole pocket with d_{xy} character at the M point in the one iron BZ is rather insensitive to doping. Finally, several Lifshitz transitions occur around Γ with doping, as expected for an iron-based superconductor and previously noted in Ref. 22. In a doping range of $0.24 < x < 0.30$, an inner hole pocket disappears, an outer hole pocket disappears, and an electron pocket ap-

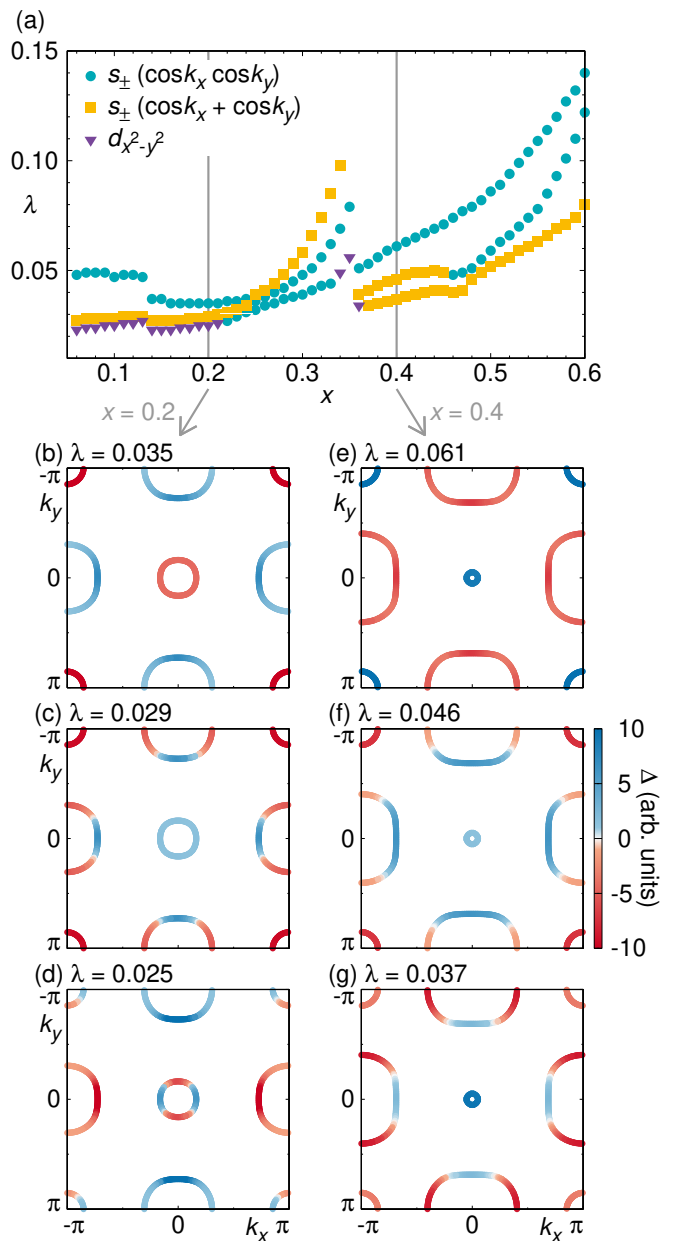


FIG. 4. (a) Leading eigenvalues λ of the gap equation as a function of doping level x . A jump is visible between $x = 0.26$ and $x = 0.27$, where both of the hole pockets around Γ disappear due to a Lifshitz transition. (b)-(d) Leading gap functions on the Fermi surface at doping $x = 0.20$. (e)-(g) The same at doping $x = 0.40$. All of the results are obtained by calculations without $\text{C}_3\text{N}_2\text{H}_{10}$.

pears; all these are of d_{xz}/d_{yz} character. The appearance of an electron pocket at Γ with doping has also been observed with ARPES on a potassium coated FeSe monolayer⁵³. Without diaminopropane molecule, the Lifshitz transitions are spread over a range $0.17 < x < 0.38$, in reasonable agreement with the DFT calculations of Ref. 22.

The main effect on the density of states at the Fermi

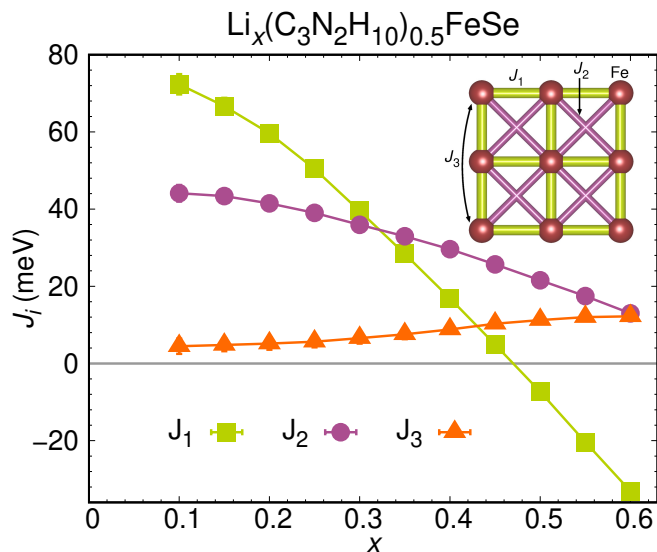


FIG. 5. Evolution of three in-plane exchange couplings of $\text{Li}_x(\text{C}_3\text{N}_2\text{H}_{10})_{0.5}\text{FeSe}$ as a function of doping x , obtained from the energy mapping technique. The inset shows the three exchange paths on the iron square lattice.

level $N(E_F)$ (shown in Ref. 51, Fig. S4) is a 30% reduction around $x = 0.27$ (or $x = 0.35$ in the calculation without $\text{C}_3\text{N}_2\text{H}_{10}$), which results from the disappearance of the two hole pockets; the appearance of the small electron pocket and its growth with doping helps $N(E_F)$ to recover.

In the series of calculations without $\text{C}_3\text{N}_2\text{H}_{10}$ molecule, we observe a doping range $0.55 < x < 0.62$, where the Fermi level is pinned to a band crossing. Topological properties of iron-based superconductors have recently been discussed intensively^{54–57}. The presence of diaminopropane molecules in a fixed position as shown in Figure 1 (a) breaks the $P4nmm$ symmetry of Li_xFeSe and leads to the opening of a small gap in the band crossing. The high symmetry may be restored on average due to the statistical distribution of molecules in the high symmetry of the $P42_12$ space group observed experimentally. Further theory and experiments are required to determine the nature of $\text{Li}_x(\text{C}_3\text{N}_2\text{H}_{10})_{0.5}\text{FeSe}$ in the doping range $0.55 < x < 0.62$. As the unfolding does not capture the $N(E_F)$ suppression in this doping range, we exclude it from our present discussion.

We now proceed to the spin fluctuation analysis by calculating the RPA spin and charge susceptibilities. As a representative example, we show in Figure 3 the diagonal components χ_{xy}^s and χ_{yz}^s for the structures with $\text{C}_3\text{N}_2\text{H}_{10}$ molecule. At low doping, the diagonal element χ_{xy}^s (Figure 3(a)) is dominated by a peak close to X and a minor peak close to M . These correspond to a nesting vector, $\mathbf{Q} = (\pi + \delta_x, 0 + \delta_y, q_z)$ connecting the electron pocket around X/Y and the hole pocket around M point, and a nesting vector $\mathbf{Q} = (\pi + \delta_x, \pi + \delta_y, q_z)$ connecting the electron pocket around X and that around Y . Further-

more, χ_{yz}^s has a peak around X , which corresponds to a nesting vector $\mathbf{Q} = (\pi + \delta_x, 0 + \delta_y, q_z)$ connecting the hole pocket around Γ and the electron pocket around X . The nesting vectors change with δ_x, δ_y because the electron pockets around X/Y grow. In both cases, the susceptibility peak formerly close to X progressively evolves towards $\mathbf{Q} = (\pi, \pi/2, q_z)$ with increasing doping. This tendency is further accentuated by the Lifshitz transition in the range $0.24 < x < 0.30$, which also rotates the orbital weights on the d_{xz}/d_{yz} hole pockets around Γ by 90 degrees.

Overall, we see an increase in both susceptibilities with doping. This is in line with the upward trend of $N(E_F)$ which is interrupted by the loss of hole pockets around $x = 0.27$ and by the band crossing pinned to the Fermi level for $0.55 < x < 0.62$. In agreement with this observation, the trend of the eigenvalue λ of the linearized gap equation as shown in Figure 4 is an increase over the entire doping range, with the exception of $x = 0.27$ where the Lifshitz transitions cause an abrupt drop of λ . The leading instabilities are different types of sign changing s wave in the whole region.

Clearly, the itinerant electron analysis of superconductivity in $\text{Li}_x(\text{C}_3\text{N}_2\text{H}_{10})_{0.5}\text{FeSe}$ presented so far can be used to explain the increasing T_c up to $x = 0.37$ observed in Ref. 22 (replotted for convenience in Ref. 51, Fig. S5) but not its suppression for higher doping. As an alternative, we now turn to the localized magnetic moment nature of the Fe $3d$ electrons to search for a mechanism to suppress superconductivity. Figure 5 shows the first three in-plane exchange couplings of $\text{Li}_x(\text{C}_3\text{N}_2\text{H}_{10})_{0.5}\text{FeSe}$ determined by energy mapping. The inspection of Heisenberg Hamiltonian parameters at this point should not be confused with the assumption of a magnetic ground state; rather, the purpose here is the analysis of the nature of the spin excitations out of which superconductivity is realized.

We find a smooth evolution of exchange couplings over the entire doping range. At small doping, the system starts with all couplings antiferromagnetic, $J_2 = 0.61J_1$ and J_3 nearly negligible. This makes the leading magnetic instability stripe-type AFM⁵¹, in perfect agreement with the weak coupling evidence of peaks at X in the spin susceptibility χ^s (Figure 3). As doping increases, J_1 decreases more rapidly than J_2 so that at $x = 0.33$, J_1 and J_2 coincide. This evolution strengthens the stripe-type AFM instability. However, the decrease of J_1 accelerates until at $x = 0.47$, J_1 crosses zero and becomes ferromagnetic. Meanwhile, J_3 is gradually increasing until at $x = 0.6$, it becomes as large as J_2 . With FM J_1 and substantial AFM J_3 , bicollinear AFM has taken over as leading magnetic instability of $\text{Li}_x(\text{C}_3\text{N}_2\text{H}_{10})_{0.5}\text{FeSe}$ (see Ref. 51, Figs. S6 and S7). Note, that in the strongly doped region, the spin susceptibilities in Figure 3 do show a peak close to $\mathbf{Q} = (\pi/2, \pi/2, 0)$ corresponding to the bicollinear order, but as this is not the dominant instability, the Heisenberg Hamiltonian cannot be understood based on the Fermi surface alone.

The bicollinear state is the magnetic ground state of FeTe, and as optimally doped $\text{FeTe}_{1-x}\text{Se}_x$ has a T_c of only 14.5 K⁵⁸, our calculation provides a strong rationalization of the falling T_c as the magnetism of $\text{Li}_x(\text{C}_3\text{N}_2\text{H}_{10})_{0.5}\text{FeSe}$ becomes more and more like that of FeTe. We identify the ferromagnetic tendencies of the nearest neighbour exchange as the key factor for determining the T_c evolution on the high doping side of the superconducting dome, outplaying all weak coupling effects of growing Fermi surfaces and growing density of states at the Fermi level.

Note that a similar transition of J_1 from AFM to FM was found for a theoretical substitution series between iron pnictides and iron germanides⁴¹, where superconductivity is in fact suppressed in the germanide. It is an interesting open question if the effect of ferromagnetic nearest neighbour interactions and thus a downward trend in T_c under electron doping could be captured in frequency dependent weak coupling methods like the fluctuation exchange approximation³⁶.

Conclusions.- We have analyzed the superconductivity of $\text{Li}_x(\text{C}_3\text{N}_2\text{H}_{10})_{0.5}\text{FeSe}$ as function of doping in the range $0.06 \leq x \leq 0.68$ both from itinerant electron and localized moment perspectives. We find that on the low doping side $x \leq 0.37$, growing Fermi surfaces

and densities of states at the Fermi level are the basis for explaining growing T_c with spin fluctuation theory. For higher doping level, weak coupling arguments would lead to the erroneous conclusion that T_c should continue to grow. However, the progressive destabilization of stripe type AFM fluctuations toward bicollinear antiferromagnetism explains why T_c decreases for $x > 0.37$. $\text{Li}_x(\text{C}_3\text{N}_2\text{H}_{10})_{0.5}\text{FeSe}$ turns out to be a perfect demonstration of the fact that iron-based superconductivity can only be understood by fully accounting for itinerant and localized aspects of the Fe $3d$ electrons. Our study highlights that in $\text{Li}_x(\text{C}_3\text{N}_2\text{H}_{10})_{0.5}\text{FeSe}$, as in many strongly correlated materials, superconductivity develops out of magnetic interactions that are high energy, not Fermi surface properties, and treating this important class of materials quantitatively calls for further refinement of theoretical methods.

ACKNOWLEDGMENTS

The authors would like to thank Hiroaki Kusunose and Igor Mazin for valuable discussions. Part of the computations were carried out at the Supercomputer Center at the Institute for Solid State Physics, the University of Tokyo.

-
- ¹ Yu. V. Pustovit and A. A. Kordyuk, Metamorphoses of electronic structure of FeSe-based superconductors, *Low Temp. Phys.* **42**, 995 (2016).
- ² A. E. Böhmer and A. Kreisel, Nematicity, magnetism and superconductivity in FeSe, *J. Phys.: Condens. Matter* **30**, 023001 (2018).
- ³ A. I. Coldea and M. D. Watson, The Key Ingredients of the Electronic Structure of FeSe, *Annu. Rev. Condens. Matter Phys.* **9**, 125 (2018).
- ⁴ T. M. McQueen, A. J. Williams, P. W. Stephens, J. Tao, Y. Zhu, V. Ksenofontov, F. Casper, C. Felser, and R. J. Cava, *Phys. Rev. Lett.* **103**, 057002 (2009).
- ⁵ M. Yi, H. Pfau, Y. Zhang, Y. He, H. Wu, T. Chen, Z. R. Ye, M. Hashimoto, R. Yu, Q. Si, D.-H. Lee, P. Dai, Z.-X. Shen, D. H. Lu, and R. J. Birgeneau, Nematic Energy Scale and the Missing Electron Pocket in FeSe, *Phys. Rev. X* **9**, 041049 (2019).
- ⁶ F.-C. Hsu, J.-Y. Luo, K.-W. Yeh, T.-K. Chen, T.-W. Huang, P. M. Wu, Y.-C. Lee, Y.-L. Huang, Y.-Y. Chu, D.-C. Yan, and M.-K. Wu, Superconductivity in the PbO-type structure α -FeSe, *Proc. Natl. Acad. Sci. (USA)* **105**, 14262 (2008).
- ⁷ E.-W. Scheidt, V. R. Hathwar, D. Schmitz, A. Dunbar, W. Scherer, F. Mayr, V. Tsurkan, J. Deisenhofer, and A. Loidl, Superconductivity at $T_c = 44$ K in $\text{Li}_x\text{Fe}_2\text{Se}_2(\text{NH}_3)_y$, *Eur. Phys. J. B* **85**, 279 (2012).
- ⁸ M. Burrard-Lucas, D. G. Free, S. J. Sedlmaier, J. D. Wright, S. J. Cassidy, Y. Hara, A. J. Corkett, T. Lancaster, P. J. Baker, S. J. Blundell, and S. J. Clarke, Enhancement of the superconducting transition temperature of FeSe by intercalation of a molecular spacer layer, *Nat. Mater.* **12**, 15 (2013).
- ⁹ S. J. Sedlmaier, S. J. Cassidy, R. G. Morris, M. Drakopoulos, C. Reinhard, S. J. Moorhouse, D. O'Hare, P. Manuel, D. Khalyavin, and S. J. Clarke, Ammonia-Rich High-Temperature Superconducting Intercalates of Iron Selenide Revealed through Time-Resolved in Situ X-ray and Neutron Diffraction, *J. Am. Chem. Soc.* **136**, 630 (2014).
- ¹⁰ P. Shahi, J. P. Sun, S. H. Wang, Y. Y. Jiao, K. Y. Chen, S. S. Sun, H. C. Lei, Y. Uwatoko, B. S. Wang, and J.-G. Cheng, High-Tc superconductivity up to 55 K under high pressure in a heavily electron doped $\text{Li}_{0.36}(\text{NH}_3)_y\text{Fe}_2\text{Se}_2$ single crystal, *Phys. Rev. B* **97**, 020508(R) (2018).
- ¹¹ W. Bao, G.-N. Li, Q.-Z. Huang, G.-F. Chen, J.-B. He, D.-M. Wang, M. A. Green, Y.-M. Qiu, J.-L. Luo, and M.-M. Wu, Superconductivity Tuned by the Iron Vacancy Order in $\text{K}_x\text{Fe}_{2-y}\text{Se}_2$, *Chin. Phys. Lett.* **30**, 027402 (2013).
- ¹² A. Krzton-Maziopa, V. Svitlyk, E. Pomjakushina, R. Puzniak, and K. Conder, Superconductivity in alkali metal intercalated iron selenides, *J. Phys. Condens. Matter* **28**, 203002 (2016).
- ¹³ H. Sun, D. N. Woodruff, S. J. Cassidy, G. M. Allcroft, S. J. Sedlmaier, A. L. Thompson, P. A. Bingham, S. D. Forder, S. Cartenet, N. Mary, S. Ramos, F. R. Foronda, B. J. Williams, X. Li, S. J. Blundell, and S. J. Clarke, Soft Chemical Control of Superconductivity in Lithium Iron Selenide Hydroxides $\text{Li}_{1-x}\text{Fe}_x(\text{OH})\text{Fe}_{1-y}\text{Se}$, *Inorg. Chem.* **54**, 1958 (2015).
- ¹⁴ X. F. Lu, N. Z. Wang, H. Wu, Y. P. Wu, D. Zhao, X. Z. Zeng, X. G. Luo, T. Wu, W. Bao, G. H. Zhang, F. Q. Huang, Q. Z. Huang and X. H. Chen, Coexistence of superconductivity and antiferromagnetism in $(\text{Li}_{0.8}\text{Fe}_{0.2})\text{OHFeSe}$, *Nat.*

- Mater. **14**, 325 (2015).
- 15 T. Noji, T. Hatakeda, S. Hosono, T. Kawamata, M. Kato, and Y. Koike, Synthesis and post-annealing effects of alkaline-metal-ethylenediamine intercalated superconductors $A_x(\text{C}_2\text{H}_8\text{N}_2)_y\text{Fe}_{2-z}\text{Se}_2$ ($A = \text{Li}, \text{Na}$) with $T_c = 45$ K, *Physica C* **504**, 8 (2014).
 - 16 X. Zhou, C. Eckberg, B. Wilfong, S.-C. Liou, H. K. Vivanco, J. Paglione, and E. E. Rodriguez, Superconductivity and magnetism in iron sulfides intercalated by metal hydroxides, *Chem. Sci.* **8**, 3781 (2017).
 - 17 L. Zheng, Y. Sakai, X. Miao, S. Nishiyama, T. Terao, R. Eguchi, H. Goto, Y. Kubozono, Superconductivity in $(\text{NH}_3)_y\text{Na}_x\text{FeSe}_{0.5}\text{Te}_{0.5}$, *Phys. Rev. B* **94**, 174505 (2016).
 - 18 C. Li, S. Su, S. Wang, and H. Lei, Enhanced superconductivity and anisotropy of $\text{FeTe}_{0.6}\text{Se}_{0.4}$ single crystals with Li-NH_3 intercalation, *Phys. Rev. B* **96**, 134503 (2017).
 - 19 S. Medvedev, T. M. McQueen, I. A. Troyan, T. Palasyuk, M. I. Erements, R. J. Cava, S. Naghavi, F. Casper, V. Ksenofontov, G. Wortmann and C. Felser, Electronic and magnetic phase diagram of $\beta\text{-Fe}_{1.01}\text{Se}$ with superconductivity at 36.7 K under pressure, *Nat. Mater.* **8**, 630 (2009).
 - 20 S. Jin, X. Fan, X. Wu, R. Sun, H. Wu, Q. Huang, C. Shi, X. Xi, Z. Lia and X. Chen, High- T_c superconducting phases in organic molecular intercalated iron selenides: synthesis and crystal structures, *Chem. Comm.* **53**, 9729 (2017).
 - 21 T. Hatakeda, T. Noji, K. Sato, T. Kawamata, M. Kato, and Y. Koike, New Alkali-Metal- and 2-Phenethylamine-Intercalated Superconductors $A_x(\text{C}_8\text{H}_{11}\text{N})_y\text{Fe}_{1-z}\text{Se}$ ($A = \text{Li}, \text{Na}$) with the Largest Interlayer Spacings and $T_c \sim 40$ K, *J. Phys. Soc. Jpn.* **85**, 103702 (2016).
 - 22 R. J. Sun, Y. Quan, S. F. Jin, Q. Z. Huang, H. Wu, L. Zhao, L. Gu, Z. P. Yin, and X. L. Chen, Realization of continuous electron doping in bulk iron selenides and identification of a new superconducting zone, *Phys. Rev. B* **98**, 214508 (2018).
 - 23 S. Hosono, T. Noji, T. Hatakeda, T. Kawamata, M. Kato, and Y. Koike, New Intercalation Superconductor $\text{Li}_x(\text{C}_6\text{H}_{16}\text{N}_2)_y\text{Fe}_{2-z}\text{Se}_2$ with a Very Large Interlayer-Spacing and $T_c = 38$ K, *J. Phys. Soc. Jpn.* **83**, 113704 (2014).
 - 24 S. Hosono, T. Noji, T. Hatakeda, T. Kawamata, M. Kato, and Y. Koike, New superconducting phase of $\text{Li}_x(\text{C}_6\text{H}_{16}\text{N}_2)_y\text{Fe}_{2-z}\text{Se}_2$ with $T_c = 41$ K obtained through the post-annealing, *J. Phys. Soc. Jpn.* **85**, 013702 (2016).
 - 25 L. Sun, X.-J. Chen, J. Guo, P. Gao, Q.-Z. Huang, H. Wang, M. Fang, X. Chen, G. Chen, Q. Wu, C. Zhang, D. Gu, X. Dong, L. Wang, K. Yang, A. Li, X. Dai, H.-K. Mao and Z. Zhao, Re-emerging superconductivity at 48 Kelvin in iron chalcogenides, *Nature* **483**, 67 (2012).
 - 26 M. Izumi, L. Zheng, Y. Sakai, H. Goto, M. Sakata, Y. Nakamoto, H. L. T. Nguyen, T. Kagayama, K. Shimizu, S. Araki, T. C. Kobayashi, T. Kambe, D. Gu, J. Guo, J. Liu, Y. Li, L. Sun, K. Prassides and Y. Kubozono, Emergence of double-dome superconductivity in ammoniated metal-doped FeSe, *Sci. Rep.* **5**, 9477 (2015).
 - 27 C.-L. Song, H.-M. Zhang, Y. Zhong, X.-P. Hu, S.-H. Ji, L. Wang, K. He, X.-C. Ma, Q.-K. Xue, Observation of Double-Dome Superconductivity in Potassium-Doped FeSe Thin Films, *Phys. Rev. Lett.* **116**, 157001 (2016).
 - 28 J. P. Sun, P. Shahi, H. X. Zhou, Y. L. Huang, K. Y. Chen, B. S. Wang, S. L. Ni, N. N. Li, K. Zhang, W. G. Yang, Y. Uwatoko, G. Xing, J. Sun, D. J. Singh, K. Jin, F. Zhou, G. M. Zhang, X. L. Dong, Z. X. Zhao and J.-G. Cheng, Reemergence of high- T_c superconductivity in the $(\text{Li}_{1-x}\text{Fe}_x)\text{OHFe}_{1-y}\text{Se}$ under high pressure, *Nat. Commun.* **9**, 380 (2018).
 - 29 J. Zhang, F.-L. Liu, T.-P. Ying, N.-N. Li, Y. Xu, L.-P. He, X.-C. Hong, Y.-J. Yu, M.-X. Wang, J. Shen, W.-G. Yang and S.-Y. Li, Observation of two superconducting domes under pressure in tetragonal FeS, *npj Quant. Mater.* **2**, 49 (2017).
 - 30 I. I. Mazin, D. J. Singh, M. D. Johannes, and M. H. Du, Unconventional superconductivity with a sign reversal in the order parameter of $\text{LaFeAsO}_{1-x}\text{F}_x$, *Phys. Rev. Lett.* **101**, 057003 (2008).
 - 31 K. Kuroki, S. Onari, R. Arita, H. Usui, Y. Tanaka, H. Kontani, and H. Aoki, Unconventional pairing originating from the disconnected Fermi surfaces of superconducting $\text{LaFeAsO}_{1-x}\text{F}_x$, *Phys. Rev. Lett.* **101**, 087004 (2008).
 - 32 P. J. Hirschfeld, M. M. Korshunov, and I. I. Mazin, Gap symmetry and structure of Fe-based superconductors, *Rep. Prog. Phys.* **74**, 124508 (2011).
 - 33 P. A. Lee, N. Nagaosa, and X.-G. Wen, Doping a Mott insulator: Physics of high-temperature superconductivity, *Rev. Mod. Phys.* **78**, 17 (2006).
 - 34 Q. Si, E. Abrahams, Strong Correlations and Magnetic Frustration in the High T_c Iron Pnictides, *Phys. Rev. Lett.* **101**, 076401 (2008).
 - 35 J. C. S. Davis and D.-H. Lee, Concepts relating magnetic interactions, intertwined electronic orders, and strongly correlated superconductivity, *Proc. Natl. Acad. Sci. U.S.A.* **110**, 17623 (2013).
 - 36 K. Suzuki, H. Usui, S. Iimura, Y. Sato, S. Matsuishi, H. Hosono, and K. Kuroki, Model of the Electronic Structure of Electron-Doped Iron-Based Superconductors: Evidence for Enhanced Spin Fluctuations by Diagonal Electron Hopping, *Phys. Rev. Lett.* **113**, 027002 (2014).
 - 37 D. Guterding, H. O. Jeschke, P. J. Hirschfeld, and R. Valentí, Unified picture of the doping dependence of superconducting transition temperatures in alkali metal/ammonia intercalated FeSe, *Phys. Rev. B* **91**, 041112(R) (2015).
 - 38 M. Shimizu, N. Takemori, D. Guterding, and H. O. Jeschke, Two-Dome Superconductivity in FeS Induced by a Lifshitz Transition, *Phys. Rev. Lett.* **121**, 137001 (2018).
 - 39 J. Hu, H. Ding, Local antiferromagnetic exchange and collaborative Fermi surface as key ingredients of high temperature superconductors, *Sci. Rep.* **2**, 381 (2012).
 - 40 J. K. Glasbrenner, I. I. Mazin, H. O. Jeschke, P. J. Hirschfeld, R.M. Fernandes, and R. Valentí, Effect of magnetic frustration on nematicity and superconductivity in iron chalcogenides, *Nat. Phys.* **11**, 953 (2015).
 - 41 D. Guterding, H. O. Jeschke, I. I. Mazin, J. K. Glasbrenner, E. Bascones, and R. Valentí, Nontrivial Role of Interlayer Cation States in Iron-Based Superconductors, *Phys. Rev. Lett.* **118**, 017204 (2017).
 - 42 K. Koepnik and H. Eschrig, Full-potential nonorthogonal local-orbital minimum-basis band-structure scheme, *Phys. Rev. B* **59**, 1743 (1999); <http://www.FPLO.de>
 - 43 J. P. Perdew, K. Burke, and M. Ernzerhof, Generalized Gradient Approximation Made Simple, *Phys. Rev. Lett.* **77**, 3865 (1996).
 - 44 H. Eschrig and K. Koepnik, Tight-binding models for the iron-based superconductors, *Phys. Rev. B* **80**, 104503 (2009).
 - 45 M. Tomić, H. O. Jeschke, and R. Valentí, Unfolding of electronic structure through induced representations of space groups: Application to Fe-based superconductors, *Phys.*

- Rev. B **90**, 195121 (2014).
- ⁴⁶ S. Graser, T. A. Maier, P. J. Hirschfeld, and D. J. Scalapino, Near-degeneracy of several pairing channels in multi-orbital models for the Fe pnictides, *New J. Phys.* **11**, 025016 (2009).
- ⁴⁷ D. Guterding, Microscopic modelling of organic and iron-based superconductors, PhD thesis, Goethe-Universität Frankfurt am Main, Germany (2017).
- ⁴⁸ H. O. Jeschke, H. Nakano, and T. Sakai, From kagome strip to kagome lattice: Realizations of frustrated $S = 1/2$ antiferromagnets in Ti(III) fluorides, *Phys. Rev. B.* **99**, 140410 (2019).
- ⁴⁹ I. I. Mazin, M. Shimizu, N. Takemori, and H. O. Jeschke, Novel Fe-Based Superconductor LaFe_2As_2 in Comparison with Traditional Pnictides, *Phys. Rev. Lett.* **123**, 267001 (2019).
- ⁵⁰ M. F. Lapa and C. L. Henley, Ground States of the Classical Antiferromagnet on the Pyrochlore Lattice, arXiv:1210.6810.
- ⁵¹ See the Supplemental material for details on the crystal structures, the electronic properties, the energy mapping and the iterative minimization calculations.
- ⁵² L. Zhao *et al.*, Common electronic origin of superconductivity in (Li,Fe)OHFeSe bulk superconductor and single-layer FeSe/SrTiO₃ films, *Nat. Commun.* **7**, 10608 (2016).
- ⁵³ X. Shi Z.-Q. Han, X.-L. Peng, P. Richard, T. Qian, X.-X. Wu, M.-W. Qiu, S. C. Wang, J. P. Hu1, Y.-J. Sun, H. Ding, Enhanced superconductivity accompanying a Lifshitz transition in electron-doped FeSe monolayer, *Nat. Commun.* **8**, 14988 (2017).
- ⁵⁴ X. Wu, S. Qin, Y. Liang, H. Fan, J. Hu, Topological characters in $\text{Fe}(\text{Te}_{1-x}\text{Se}_x)$ thin films, *Phys. Rev. B* **93**, 115129 (2016).
- ⁵⁵ G. Xu, B. Lian, P. Tang, X.-L. Qi, S.-C. Zhang, Topological Superconductivity on the Surface of Fe-Based Superconductors, *Phys. Rev. Lett.* **117**, 047001 (2016).
- ⁵⁶ P. Zhang, K. Yaji, T. Hashimoto, Y. Ota, T. Kondo, K. Okazaki, Z. Wang, J. Wen, G. D. Gu, H. Ding, S. Shin, Observation of topological superconductivity on the surface of an iron-based superconductor, *Science* **360**, 182 (2018).
- ⁵⁷ D. Wang, *et al.*, Evidence for Majorana bound states in an iron-based superconductor, *Science* **362**, 333 (2018).
- ⁵⁸ N. Katayama, S. Ji, D. Louca, S. Lee, M. Fujita, T. J. Sato, J. Wen, Z. Xu, G. Gu, G. Xu, Z. Lin, M. Enoki, S. Chang, K. Yamada, J. M. Tranquada, Investigation of the Spin-Glass Regime between the Antiferromagnetic and Superconducting Phases in $\text{Fe}_{1+y}\text{Se}_x\text{Te}_{1-x}$, *J. Phys. Soc. Jpn.* **79**, 113702 (2010).

Importance of Fermi surface and magnetic interactions for the superconducting dome in electron doped FeSe intercalates

– Supplemental Material –

Makoto Shimizu,¹ Nayuta Takemori,² Daniel Guterding,³ and Harald O. Jeschke²

¹*Department of Physics, Okayama University, Okayama 700-8530, Japan*

²*Research Institute for Interdisciplinary Science, Okayama University, Okayama 700-8530, Japan*

³*Fachbereich Mathematik, Naturwissenschaften und Datenverarbeitung,*

Technische Hochschule Mittelhessen, Wilhelm-Leuschner-Straße 13, 61169 Friedberg, Germany

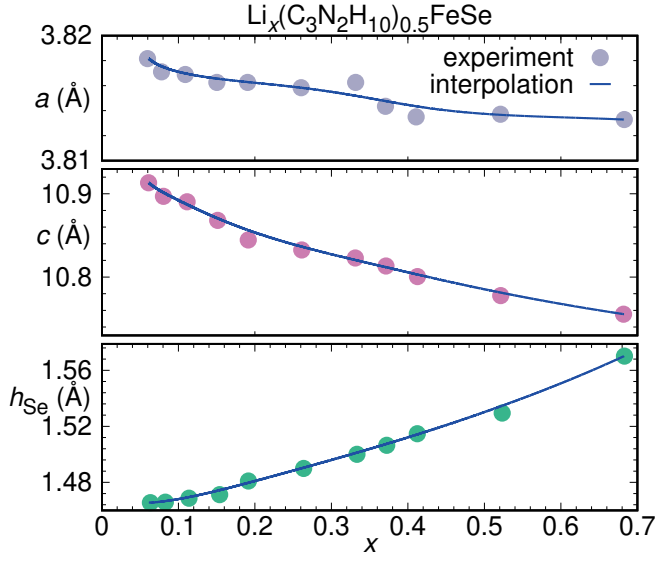


FIG. S1. Structural parameters from Ref. 1 (symbols) and interpolation (lines). Calculations were performed for interpolated structures in steps of $\Delta x = 0.01$.

I. CRYSTAL STRUCTURES

The study of $\text{Li}_x(\text{C}_3\text{N}_2\text{H}_{10})_{0.37}\text{FeSe}$ requires preparation of model structures as the experimental crystal structure provided in Ref. 1 contains some disorder and is not directly amenable to DFT calculations. First of all, the diaminopropane molecule is placed on an $8g$ Wyckoff position of the $P4_212$ space group with partial occupancy of 0.093, leading to 0.372 $\text{C}_3\text{N}_2\text{H}_{10}$ molecules per FeSe. We simplify this structure by lowering the symmetry to $P1$ and by picking one of the eight symmetry equivalent $\text{C}_3\text{N}_2\text{H}_{10}$ molecules. This leads to the approximate stoichiometry $\text{Li}_x(\text{C}_3\text{N}_2\text{H}_{10})_{0.5}\text{FeSe}$. This structure is shown in Figure 1 of the main text. Note that Sun *et al.* show a very similar simplified structure¹. The simplification is justified because the diaminopropane molecules are important for fixing the interlayer distance; however, electronically, the highest occupied molecular orbitals are significantly below the Fermi level while the lowest unoccupied molecular orbital is slightly above the Fermi level so that the molecules are not active at the Fermi level. In order to obtain a finely spaced series of crystal

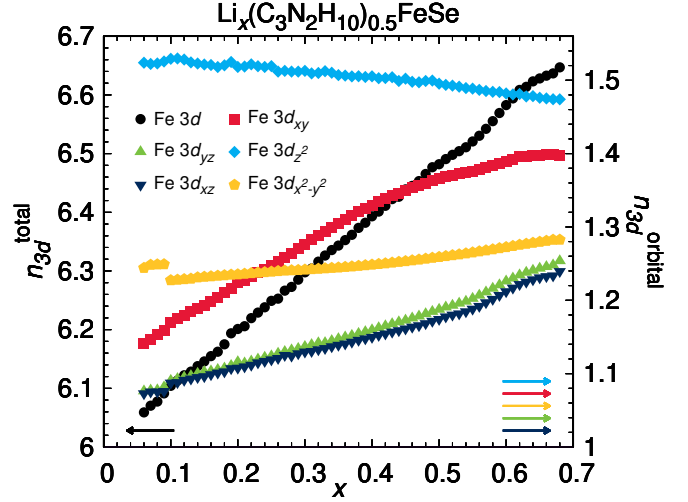


FIG. S2. Evolution of the total and orbital resolved Fe $3d$ occupation number as a function of doping.

structures of $\text{Li}_x(\text{C}_3\text{N}_2\text{H}_{10})_{0.5}\text{FeSe}$ as a function of doping level x , we interpolate the structural data provided in Ref. 1 as shown in Figure S1. This guarantees that we do not incur the well-known difficulties of predicting the chalcogenide z position in iron chalcogenide superconductors. Combining the diaminopropane molecule coordinates given for $x = 0.26$ with the lattice parameters of Figure S1 would lead to expanded or compressed molecules as a function of doping. This would be unrealistic as the molecules remain approximately neutral over the whole doping range, and their bonds should be rigid. Therefore, we adapt the diaminopropane molecule Wyckoff positions to the changing lattice parameters, keeping all distances and angles within the molecules constant. We model the doping x by using the virtual crystal approximation for Li, using a nuclear charge between neon and lithium of $Z = 2 + x$.

II. ELECTRONIC PROPERTIES

In Figure S3, we show the unfolded one iron Fermi surfaces of Li_xFeSe with $\text{C}_3\text{N}_2\text{H}_{10}$ molecules for six doping levels. The corresponding Fermi surfaces of $\text{Li}_x(\text{C}_3\text{N}_2\text{H}_{10})_{0.5}\text{FeSe}$ are shown in the main

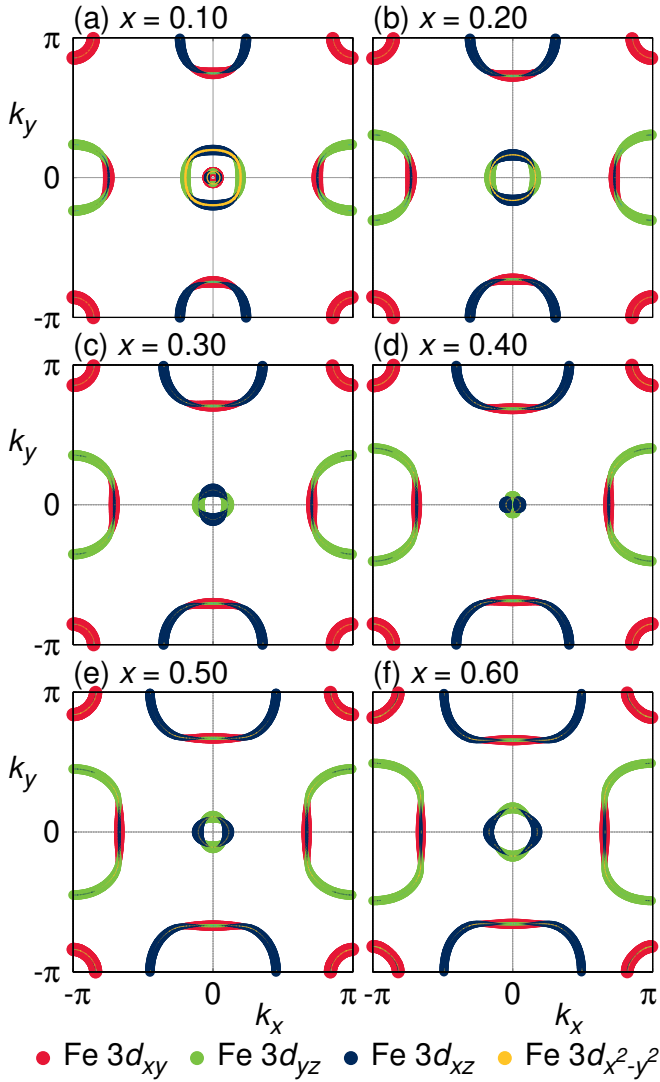


FIG. S3. Evolution of the Fermi surface at $k_z = 0$ with doping for Li_xFeSe without $\text{C}_3\text{N}_2\text{H}_{10}$ molecule. The Fe 3d orbital weights are indicated by color. Orbital weight of Fe $3d_{z^2}$ at the Fermi level is nearly negligible.

text. In Figure S2, we show electron densities of $\text{Li}_x(\text{C}_3\text{N}_2\text{H}_{10})_{0.5}\text{FeSe}$ as a function of doping levels $0.06 \leq x \leq 0.68$. The data are obtained by integrating iron total and orbital resolved densities of states up to the Fermi level.

Figure S4 shows the density of states at the Fermi level $N(E_F)$ with and without $\text{C}_3\text{N}_2\text{H}_{10}$ molecule. $N(E_F)$ of the ten-band tight binding model faithfully represents the DFT result. On the other hand, there is some deviation for the unfolded five-band tight binding model for larger dopings, and in particular in the range $0.55 < x < 0.62$ as discussed in the main text. These deviations stem from the dopants, which lower the crystal symmetry compared to pristine FeSe, so that the unfolding to the five band model becomes only approximate.

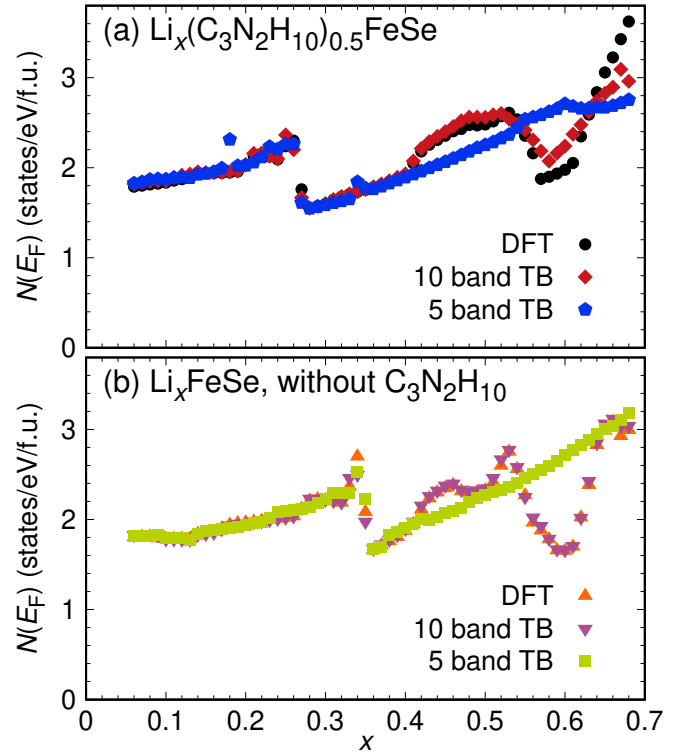


FIG. S4. Density of states at the Fermi level $N(E_F)$ for the two series of structures used in this study. (a) Full structure with diaminopropane molecule, (b) Li_xFeSe with empty van der Waals gap.

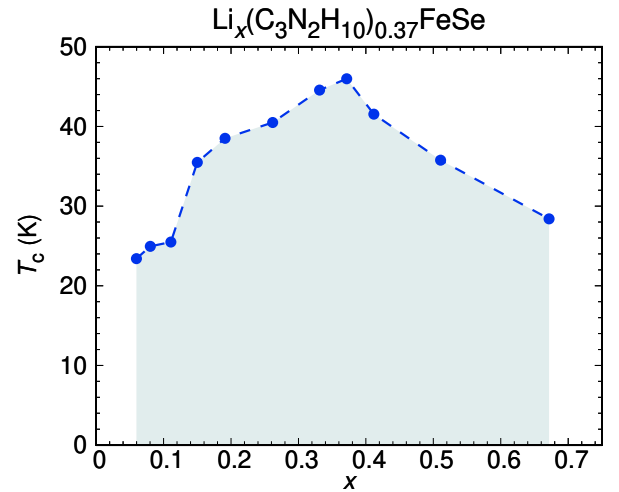


FIG. S5. Superconducting T_c of $\text{Li}_x(\text{C}_3\text{N}_2\text{H}_{10})_{0.5}\text{FeSe}$ as a function of doping, as reported in Ref. 1.

III. ENERGY MAPPING

The exchange couplings of $\text{Li}_x(\text{C}_3\text{N}_2\text{H}_{10})_{0.5}\text{FeSe}$ were determined by the energy mapping technique^{2,3}. They are listed in Table S1. $2 \times 2 \times 1$ supercells with $P1$ symmetry contain eight inequivalent iron sites, allowing for 13 spin configurations with different energies. Two exam-

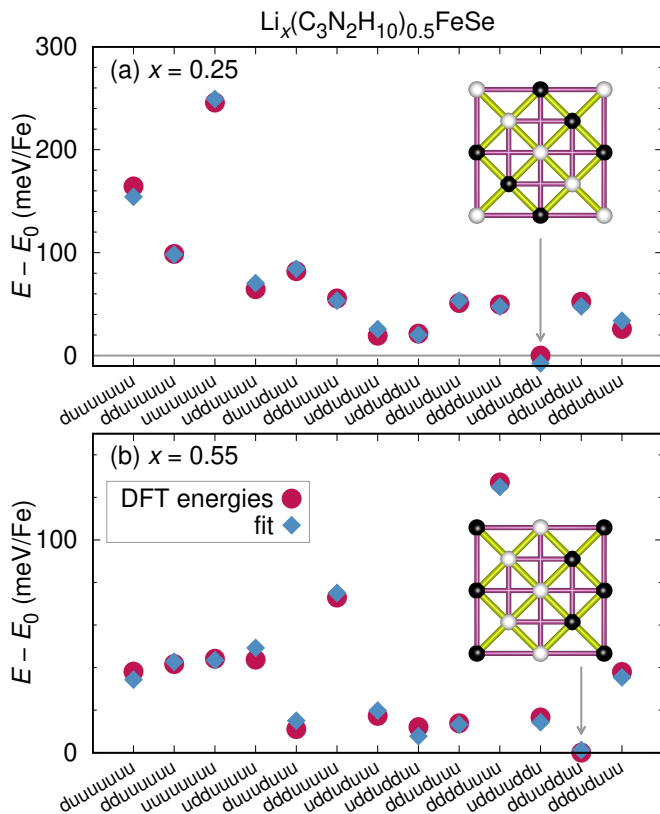


FIG. S6. Two examples for the energy mapping of $\text{Li}_x(\text{C}_3\text{N}_2\text{H}_{10})_{0.5}\text{FeSe}$ at (a) $x = 0.25$ and (b) $x = 0.55$. In both panels the inset shows an eight iron supercell with the minimum energy spin configuration marked by white for up and black for down. Up to a doping of $x = 0.45$, the stripe-type order is lowest in energy, while from $x = 0.5$, the bicollinear order is stabilized.

ples are shown in Figure S6. Due to the metallic nature of the FeSe intercalate, the fit to the DFT energies is not as good as in magnetic insulators⁴ but it is very reasonable as indicated by the small deviations between fitted and DFT energies and by the small error bars shown in Figure 5 of the main text. Note that at large doping, the bicollinear configuration takes over from stripe-type as lowest energy spin configuration (Figure S6).

IV. ITERATIVE MINIMIZATION METHOD

The iterative minimization method allows the efficient determination of ground state spin configurations of classical spin systems^{5,6}. We use this method to obtain the ground states of the classical Heisenberg models with the exchange couplings in Table S1. We Fourier transform the obtained spin configurations to obtain the spin structure factor $S(\mathbf{q})$. The spin structure factors of $\text{Li}_x(\text{C}_3\text{N}_2\text{H}_{10})_{0.5}\text{FeSe}$ for doping values $x = 0.10$ and $x = 0.60$ are shown in Fig. S7. In the doping region of $0.10 \leq x \leq 0.45$, we find peaks at $\mathbf{q} = (\pi, 0)$ or $\mathbf{q} = (0, \pi)$,

TABLE S1. Exchange couplings of $\text{Li}_x(\text{C}_3\text{N}_2\text{H}_{10})_{0.5}\text{FeSe}$, calculated with GGA and $4 \times 4 \times 4$ k points. The errors shown are only the statistical error arising from the energy mapping.

x	J_1 (meV)	J_2 (meV)	J_3 (meV)
0.1	72.3(2.7)	44.1(2.2)	4.5(2.0)
0.15	66.7(2.2)	43.4(1.8)	4.8(1.7)
0.2	59.7(2.1)	41.5(1.7)	5.1(1.6)
0.25	50.4(2.0)	39.0(1.6)	5.7(1.5)
0.3	39.5(1.9)	35.9(1.6)	6.6(1.5)
0.35	28.4(1.7)	33.0(1.4)	7.6(1.3)
0.4	16.9(1.4)	29.6(1.1)	8.8(1.0)
0.45	4.9(1.1)	25.7(9)	10.3(8)
0.5	-7.3(1.0)	21.6(8)	11.2(8)
0.55	-20.4(1.1)	17.5(9)	12.0(9)
0.6	-33.1(1.1)	13.0(9)	12.2(8)

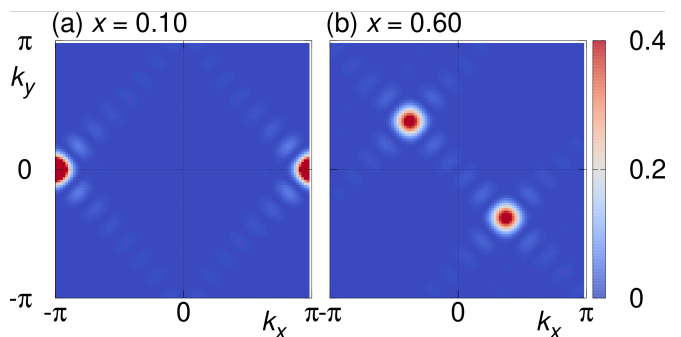


FIG. S7. Spin structure factors $S(\mathbf{q})$ at $x = 0.10$ and $x = 0.60$, obtained by Fourier transforming the ground state spin configuration found with iterative minimization.

indicating stripe AFM order as ground states. On the other hand, for $0.50 \leq x \leq 0.60$, as soon as J_1 turns ferromagnetic, we find peaks at $\mathbf{Q} = (q, q)$ where $q \sim 0.4\pi$. As it is well known that FeSe also has a substantial bi-quadratic coupling⁷ which we do not re-determine here, the highly doped $\text{Li}_x(\text{C}_3\text{N}_2\text{H}_{10})_{0.5}\text{FeSe}$ samples will actually be in the bicollinear phase with $\mathbf{q} = (\pi/2, \pi/2)$ and magnetically resemble FeTe.

¹ R. J. Sun, Y. Quan, S. F. Jin, Q. Z. Huang, H. Wu, L. Zhao, L. Gu, Z. P. Yin, and X. L. Chen, Realization of continuous

electron doping in bulk iron selenides and identification of a

- new superconducting zone, *Phys. Rev. B* **98**, 214508 (2018).
- ² H. O. Jeschke, I. Opahle, H. Kandpal, R. Valentí, H. Das, T. Saha-Dasgupta, O. Janson, H. Rosner, A. Brühl, B. Wolf, M. Lang, J. Richter, S. Hu, X. Wang, R. Peters, T. Pruschke, and A. Honecker, Multi-step approach to microscopic models for frustrated quantum magnets: The case of the natural mineral azurite, *Phys. Rev. Lett.* **106**, 217201 (2011).
- ³ H. O. Jeschke, H. Nakano, and T. Sakai, From kagome strip to kagome lattice: Realizations of frustrated $S = 1/2$ antiferromagnets in Ti(III) fluorides, *Phys. Rev. B* **99**, 140410 (2019).
- ⁴ Y. Iqbal, T. Müller, K. Riedl, J. Reuther, S. Rachel, R. Valentí, M. J. P. Gingras, R. Thomale, H. O. Jeschke, Signatures of a gearwheel quantum spin liquid in a spin- $1/2$ pyrochlore molybdate Heisenberg antiferromagnet, *Phys. Rev. Mater.* **1**, 071201(R) (2017).
- ⁵ M. F. Lapa and C. L. Henley, Ground States of the Classical Antiferromagnet on the Pyrochlore Lattice, arXiv:1210.6810.
- ⁶ Y. Iqbal, T. Müller, H. O. Jeschke, R. Thomale, and J. Reuther, Stability of the spiral spin liquid in MnSc_2S_4 *Phys. Rev. B* **98**, 064427 (2018).
- ⁷ J. K. Glasbrenner, I. I. Mazin, H. O. Jeschke, P. J. Hirschfeld, R.M. Fernandes, and R. Valentí, Effect of magnetic frustration on nematicity and superconductivity in iron chalcogenides, *Nat. Phys.* **11**, 953 (2015).